Millennial-scale Atlantic/East Pacific sea surface temperature linkages during the last 100,000 years.

Nathalie Dubois[a,b*], Markus Kienast[c], Stephanie S. Kienast[c], Axel Timmermann[d]

[a]Woods Hole Oceanographic Institution, 266 Woods Hole Road, MA, 02543, USA

[b]Present address: Eawag, Überlandstasse 133, 8600 Dübendorf, Switzerland

[c]Dalhousie University, 1255 Oxford Street, Halifax, NS, B3H 4J1, Canada

[d]International Pacific Research Center, University of Hawaii, 2525 Correa Road, HI 96822, USA

*Corresponding author: nathalie.dubois@eawag.ch

Abstract

Amplifying both internally generated variability and remote climate signals from the Atlantic Ocean via coupled air-sea instabilities, the eastern tropical Pacific (ETP) is well situated to detect past climate changes and variations in Central American wind systems that dynamically link the Atlantic and the Pacific.

Here we compare new and previously published alkenone-based sea surface temperature (SST) reconstructions from diverse environments within the ETP, i.e. the Eastern Pacific Warm Pool (EPWP), the equatorial and the northern Peruvian Upwelling regions over the past 100,000 years. Over this time period, a fairly constant meridional temperature gradient across the region is observed, indicating similar hydrographic conditions during glacial and interglacial periods. The data further reveal that millennial-scale cold events associated with massive iceberg surges in the North Atlantic (Heinrich events) generate cooling in the ETP from ~8°N to ~2°S. Data from Heinrich event 1 however indicate that the response changes sign south of 2°S. These millennial-scale alterations of the SST pattern across diverse environments of the ETP support previous climate modeling experiments that suggested an Atlantic-Pacific connection caused by the intensification of the Central American gap winds, enhanced upwelling and mixing north of the equator and supported by positive air-sea feedbacks in the eastern tropical Pacific.

Keywords: Eastern Pacific, Heinrich Events, Winds, Sea Surface Temperature, Alkenone, EOF

1. Introduction

The ETP is home to the El Niño-Southern Oscillation (ENSO) phenomenon, which affects weather and climate patterns worldwide. Recent studies on remote triggers of ETP climate variability have suggested possible extratropical atmospheric influences (Alexander et al., 2010; Caballero and Anderson, 2009; Vimont et al., 2003), along with potential effects from tropical Atlantic SSTs (Okumura et al., 2009; Timmermann et al., 2007; Zhang and Delworth, 2005). Given the limited degrees of freedom in the short instrumental record, the Atlantic/tropical Pacific linkage is difficult to establish with statistical confidence. Paleo-climate data could provide additional insight into the mechanisms that communicate Atlantic climate anomalies into the tropical Pacific. Moreover, understanding this pan-oceanic atmospheric bridge and the associated changes in moisture transport across Central America (Leduc et al., 2007; Richter and Xie, 2010) will shed further light on the long-term behavior and stability of the Atlantic Meridional Overturning Circulation vis-à-vis Deep Water Formation in the North Pacific (Okazaki et al., 2010).

Here we compare three ETP alkenone-based SST reconstructions of the past 100,000 years that document a recurring link between Atlantic and Pacific climate on millennial timescales, thus extending previous studies that identified a connection between Atlantic climate change, Pacific hydroclimate variability (Benway et al., 2006; Leduc et al., 2007; Pahnke et al., 2007) and Pacific SSTs (Kienast et al., 2006; Pahnke et al., 2007; Koutavas and Sachs, 2008) during the last glacial termination. We perform empirical orthogonal function (EOF) analyses of these three 100,000 years long SST records and of a compilation of eleven previously published alkenone-based SST records from the ETP covering the last 25,000 years.

2. Regional setting

The ETP is characterized by prominent climatic asymmetries and large seasonal variations in wind patterns, surface currents, temperature and salinity. North of the equator, the EPWP is characterized by annual mean temperatures exceeding 27.5°C and exceptionally low salinities (~32 practical salinity units, psu), resulting from intense rainfall associated with the Intertropical Convergence Zone (ITCZ) and atmospheric water vapor export from the Caribbean across the Panama Isthmus (Joussaume et al., 1986; Mitchell and Wallace, 1992; Li and Philander, 1996; Xie et al., 2005) via the northeasterly trade winds (Fig. 1).

Straddling the equator on the other side are the southeasterly trade winds that converge into the northern hemisphere ITCZ. These winds cause Ekman divergence along the equator and give rise to the equatorial Cold Tongue (mean SST of 24°C, Fig. 1d). The southeasterly trades also cause upwelling off the coast of Peru. The Peru Current advects cold coastal waters into the far eastern tropical Pacific, thus contributing to the low temperatures in the Cold Tongue region.

The seasonal cycle of ETP SST and ocean currents is linked to the seasonal meridional migration of the ITCZ (Fig. 1 a-d). During present-day boreal summer & autumn (May to late November), when the ITCZ is in its northernmost position (10-12°N, Fig. 1b), the southerly winds are strongest over the equator and the Equatorial and Peruvian Upwelling intensify (Fig. 1d; Wyrtki, 1981). A strong meridional SST gradient develops across the equator, between the EPWP and the Cold Tongue with a well-pronounced Equatorial Front near 2–5ºN (Wyrtki, 1996; Pak and Zaneveld, 1974). At the equator, SSTs are at their minimum in September (Fig. 1d).

This stage is contrasted by conditions in boreal winter and spring (December to April), when the ITCZ is at its most equatorial position, strong northeasterly trades cross the Central American Isthmus (Fig. 1a) and southeast trade winds and the equatorial Cold Tongue are relatively weak (Fig. 1c; Li and Philander, 1996). SSTs reach their maximum in March. As the strong northeasterly trades accelerate through topographic gaps in the Central American Cordillera, they form smaller-scale features known as the Tehuantepec, Papagayo and Panama wind jets (Fig. 1a; Xie et al., 2005; Chelton et al., 2000). The wind stress curl associated with these jets causes localized upwelling, thermocline changes and SSTs minima extending off the coast off Central America (Fig. 1a and 1c; Kessler, 2002; Xie et al., 2005; Willett et al., 2006). Of particular importance is the Panama Jet (January to April) which generates a cold SST patch in its wake (Fig. 1c) that can inhibit convection and breaks the winter ITCZ into two parts (Alory et al., 2012). The Papagayo Jet and its related wind stress curl pattern create the so-called Costa Rica Dome, an oceanic upwelling center where the thermocline ascends to very near the sea surface (Fiedler, 2002; Kessler, 2006). A local SST minimum at 9°N, 89°W marks the Costa Rica Dome (Fig.1c), which ranges in diameter from 100 to 900 km. These gap winds (i.e., winds that are accelerated by an along-gap pressure gradient) have been associated with variations in the Caribbean trade winds (Frankenfield, 1917) and high pressure systems of midlatitude origin that move southeastward across the Gulf of Mexico (a.k.a. “Northers” or “Central American Cold Surges”; Schultz et al., 1997; 1998).

3. Material

Here we present an extended 100 kyr-long record of alkenone-based (UK'37-) SST reconstructions from core ME0005A-43JC (hereafter ME43) collected off the Costa Rican margin in the EPWP (Fig. 1a). We compare this record with two UK'37-SST reconstructions from the equatorial Cold Tongue environment (ME0005A-24JC and ME0005A-27JC, hereafter ME24 and ME27, respectively), recently published by Dubois et al. (2011). Note that Kienast et al. (2006) recently published SST reconstructions from the last 25 kyr for ME24 and Dubois et al. (2009) for ME27 and ME43.

3.1 Core locations

Core ME43 (7°51.35'N, 83°36.50'W, 1368 m water depth) was collected during the ME0005A expedition aboard the *R/V Melville* in 2000, off the Costa Rican margin in the EPWP. Sediment cores ME24 (0°01'N, 86°27'W, 2941 m water depth) and ME27 (1°51'S, 82°47'W, 2203 m water depth) were recovered during the same expedition as core ME43. The strategic location of these cores across this complex oceanographic region is ideal to detect hydrographic changes (Fig. 1). As shown in the main text, both coastal and equatorial upwelling systems co-exist in the ETP. Our southernmost core site ME27 is affected partly by the highly productive waters originating from of the coastal upwelling region off Peru, where deep subantarctic-sourced, nutrient-rich water are upwelling that originate from the deeper part of the Equatorial Under Current (EUC). Core ME24 is situated within the Equatorial Upwelling zone, where shallower waters from the upper EUC branch reach the surface via the equatorial divergence (Dugdale et al., 2004). The local hydrology at our northern most core site ME43 is not affected by local upwelling dynamics, as it is situated in the lee of the Talamanca Cordillera, which reaches altitudes of 3,000 to 4,000 m above sea level (Chelton et al., 2000). At this core location, mean annual SST is higher than 28°C (Benway et al., 2006). However, site ME43 is situated in-between the Costa Rica Dome and the SST minimum associated with the Panama Jet (Fig. 1c), and may be sensitive to intensification of either of these upwelling centers.

3.2 Age models

All age models are based on previously published planktonic foraminifera radiocarbon dates collected via accelerator mass spectrometry (AMS), benthic oxygen isotope stratigraphy, and the detection of the Los Chocoyos Ash Layer (Drexler et al., 1980) in ME24 and ME27 (see Tables 1-2 and Fig. 2 for details and data sources). We updated the age models for all three cores using the recently published MARINE13 calibration data set (Reimer et al., 2013). All radiocarbon dates were converted to calendar ages using the Calib 7.0 program. For ME43, a reservoir age of 558 years, the regional average for the west coast of Central America (Stuiver and Reimer, 1993) was employed. For ME24 and ME27, a reservoir age of 467 years was employed. The calendar age with the median probability was selected (Table 1). Age models were created by linearly interpolating between derived calendar ages.

Age model for core ME43 was updated from Benway et al. (2006). The use of a new calibration data set (MARINE13) only leads to small deviations (<450 yr) from the calendar ages published by Benway et al. (2006) using MARINE04 (Hughen et al., 2004;

See Table 1). Note that for the interval 23-85 kyr BP, Benway et al. (2006) correlated 3 planktonic $\delta^{18}O$ tie points to GISP2 $\delta^{18}O$ (Grootes and Stuiver, 1997) and 6 benthic $\delta^{18}O$ tie points to MD95-2042, a core from the Iberian Margin (MD95-2042, 37°48'N, 10°10'W) whose stratigraphy was based on correlating planktonic $\delta^{18}O$ to GRIP $\delta^{18}O$ (Shackleton et al., 2000). Here we chose to correlate all three benthic oxygen isotope records (A. Mix, unpubl. data) to the benthic stack LR04 (Lisiecki and Raymo, 2005; See Fig. 2). This leads to small changes in the original ME43 age model, reaching a maximum of 1.4 kyr around 46 and 54 kyr BP (Fig. 2 and Table 2). These results are available from the National Climatic Data Center at http://www.ncdc.noaa.gov/data-access/paleoclimatology-data/datasets/paleoceanography.

As pointed out in previous studies, the assumption of a constant reservoir age in radiocarbon dating is challenging, especially in upwelling regions, given the likelihood of variations in upwelling intensity and exchange with the atmosphere (Marchitto et al., 2007; Singarayer et al., 2008). While we acknowledge the potential chronological error associated with this uncertainty, we do not yet have the ability to account for this.

The temporal resolution of core ME43 is one sample every 400 years on average for the last 30 kyr, and 1 sample every 610 years on average for the interval 30-100 kyr BP. Cores ME24 and ME27 have similar resolution with - on average - one sample every 340 years and one sample every 650 years, respectively.

4. Methods

4.1 Laboratory analysis

Core ME43 was analyzed for alkenone unsaturation at Dalhousie University. Total lipids were extracted from 1.5 to 3 g aliquots of freeze-dried sediment samples using a Dionex Accelerated Solvent Extraction system (ASE200). These extracts were saponified using potassium hydroxide and purified through silica column chromatography. The purified extracts were analyzed by gas chromatography (Agilent 6890N) at Dalhousie. The UK’37 index was calculated according to the relative concentrations of the di- and tri-unsaturated C37 alkenones: UK′37 = [C37:2]/[C37:2 + C37:3]. Sea-surface temperature estimates (UK’37-SST) were calculated from the ratio of the concentration of the di- and triunsaturated alkenones, using the calibration of Prahl et al. (1988): SST (°C) = (UK’37-0.039)/0.034. This calibration has recently been shown to best relate alkenone unsaturation to sea surface temperatures in the ETP (Kienast et al., 2012). Based on replicate analysis, the analytical precision of the method is ±0.01 UK′37 units (0.3°C). The standard calibration error is estimated at ±1.5°C. These results are available from the National Climatic Data Center at http://www.ncdc.noaa.gov/data-access/paleoclimatology-data/datasets/paleoceanography.

4.2 Empirical orthogonal functions

Empirical orthogonal function (EOF) analyses are performed here on two different compilations of UK’37-SST reconstructions of the ETP, abbreviated as vector $\mathbf{T}(t)=(T_i(t))$. The first one is based on the SST reconstructions of cores ME43, ME24 and ME27 and covers the period from 100 to 5 kyr BP. The second one is performed on a set of recently published alkenone-based SST reconstructions from the ETP and covers the last deglacial period (25-5 kyr BP).

EOF analysis is a commonly used statistical method that determines the leading orthogonal patterns (denoted as $\mathbf{e}_i$) of variability of a multivariate dataset $\mathbf{T}(t)$ and their corresponding principal components $p_i(t)$, such that $\mathbf{T}(t)=\Sigma_i\ p_i(t)\ \mathbf{e}_i$. The corresponding principal component $p_i(t)$ can be expressed as the scalar product $p_i(t)=\mathbf{T}(t)\bullet\mathbf{e}_i$. The contribution of each EOF to the SST evolution at a sediment core location is determined by multiplying the corresponding principal components with the EOF pattern loading at this site. EOF patterns are ranked based on their explained variance to the total multivariate dataset. Prior to the EOF analysis all the SST reconstructions were linearly interpolated onto the same equidistant time grid with a grid spacing of 100 years. Locations of the ETP cores used in the deglacial EOF computation are given in Table 3, along with the actual EOF values for each core. Original UK'37-SST reconstructions used in the deglacial EOF are shown in Fig. 3. Note that we have used an updated age model for core V19-30, as presented by Kienast et al. (2013).

5. Results

5.1 UK'37-SST reconstructions

All three SST records reveal a long-term cooling trend from 100 to 17 kyr BP, followed by a more rapid warming during the deglaciation and the Holocene (Fig. 4b-d). The dominant glacial/interglacial SST magnitude ranges from 1.5°C-2.5°C. A striking feature revealed by all three data sets is an unusually warm period (80-100 kyr BP) during MIS5, with temperatures exceeding those of the Holocene by up to 1°C.

To determine the spatial inhomogeneity of orbital-scale variability we calculated the SST differences between the sites (ΔSST, Fig. 4f-h). In order to avoid large amplitude variability due to age model uncertainties and outlier samples, we computed the ΔSST after a 15 points smoothing of the SST curves re-sampled at 500 years intervals (Fig. 4b-d). We find that the low-frequency temperature gradients between the 3 sites remain relatively stable through the last 100 kyr varying by no more than +/- 1°C. A slight long-term increase in the gradient between the EPWP and Cold Tongue can be observed in Fig. 4g and h (ME43-ME24 and ME43-ME27).

Millennial-scale oscillations are superimposed on this long-term trend, with highest amplitudes during MIS3. Dubois et al. (2011) noticed that the SST difference between ME24 and ME27, both located in the Cold Tongue region remains relatively constant over the last 100 kyr, except during rapid and pronounced millennial-scale cooling intervals during which the SST gradient is minimal. Interestingly, the SST record of ME43, located further north in the EPWP, reveals millennial-scale cooling intervals that appear to coincide within dating uncertainty with the cooling events observed in the Cold Tongue. Note that the ΔSST records in Fig. 4f-h cannot be used to infer millennial-scale changes between the cores since these records have been smoothed.

5.2 EOF analysis

To identify the leading patterns of orbital and millennial-scale variability during the last glacial period, we computed the leading Empirical Orthogonal Function ("long-term" EOF) mode of the linearly interpolated SST records ME24, ME27 and ME43. The first mode explains 93.7% of the joint variance for these three cores and shows a monopole pattern of EOF loadings (Fig. 5a). The corresponding principal component (Fig. 4e, 5d) is characterized by the large-scale glacial signal and millennial-scale variability. Millennial-scale features in this mode coincide with the exceptionally cold stadials in northeastern

North Atlantic SST (Fig. 5d, blue line) and the associated periods of iceberg surging (Heinrich events) H1, H2, H4, H5 and H6. H3 is not evident and H4 is not well marked in our Pacific SST records. However, the interpretation of ETP sedimentary records is complicated by the fact that they are of lower temporal resolution and affected by local processes. While there is thus no one-on-one match between North Atlantic/Greenland events and the ETP paleoceanographic events presented here, we nevertheless interpret the cooling in the ETP during H1, H2, H4, H5 and H6 to be indicative of a strong linkage between the Atlantic and the ETP.

This Atlantic/Pacific linkage is further corroborated by a deglacial EOF analysis of eleven ETP SST reconstructions covering the period of the last glacial termination and the early Holocene. For this analysis we used UK'37-based SST from cores V19-27, V19-28, V19-30, V21-30, RC11-238, MD02-2529, JPC32-14, ME24, ME27, ME43 and TR31 (See Table 3 for locations and original references). Note that this set of cores is located between 8.1°N and 3.3°S and thus extends further south than the longer cores ME43, 24 and 27. Figure 5 shows the 1st and 2nd deglacial EOF modes ($\mathbf{e}_{1,}$ $\mathbf{e}_2$) and their corresponding principal components ($p_1(t)$, $p_2(t)$). The leading deglacial SST mode in the ETP, explaining 80.5% of the total variance, is also monopole pattern (Fig. 5b). Its time-evolution is characterized by a cooling during Heinrich event 1 (H1, 17-15 kyr BP), a relatively fast warming at around 15.5 kyr BP, a stalling of temperatures during the Younger Dryas (YD) period and a subsequent gradual temperature rise into the mid Holocene (Fig. 5e). The second EOF mode of deglacial temperatures in the ETP explains 10.0% of the variance and reveals a N-S dipole pattern (Fig. 5c). Its time-evolution is characterized by cooling during both H1 and H2 (Fig. 5f).

6. Discussion

6.1 Orbital-scale variations in ETP SST

As shown in Figure 4, the temperature gradients between the 3 long-term records remain relatively stable throughout the last 100 kyr. This near-stationary temperature offset between the EPWP, the Equatorial Upwelling and the northern Peru Upwelling regions over the last 100 kyrs suggests that the dynamics regulating SST on glacial-interglacial timescales affected these environments uniformly. However, a slight long-term increase in the gradient between the EPWP (ME43) and Cold Tongue (ME27 and ME24) can be observed in Fig. 4f and 5g (between 100 and 15 kyr BP). Furthermore, the larger glacial (MIS2-4) gradient between the two Cold Tongue sites (Fig. 4h) suggests a stronger cooling in the Peru Upwelling (ME27) relative to the Equatorial Upwelling environment. This observation supports previous findings of enhanced advection in the Peru Current during glacials compared to interglacials (Kaiser et al., 2005; Dubois et al., 2009).

The leading deglacial principal component (Fig. 5b and e) exhibits a monopole pattern, most probably controlled simultaneously by different local and remote forcings. Figure 5e suggests that although CO_2 is already increasing at 18 kyr BP (blue curve in Fig. 5e), PC1 does not increase until 15.5 kyr BP partly because it is compensated for by the drop in solar insolation in the boreal fall (October, November, December, OND, orange dashed curve in Fig. 5e) and the resulting temperature effect in December, January, February (DJF). Note: SSTs in the ETP lag the annual cycle insolation forcing and its modulation through the Milankovitch cycles by about 2 months. This lag emerges from the mean mixed layer depth of about 30m and a thermal damping timescale of about 3 −

4 months (Barnett et al., 1991).

6.2 Millennial-scale variability in the ETP

Most research on suborbital timescales in the Eastern Pacific focused on the hydrologic cycle and sea surface salinity variations (e.g. Benway et al., 2006; Leduc et al., 2007; Pahnke et al., 2007). Significant disparities emerged and were already discussed by Pahnke et al. (2007) and Prange et al. (2010), highlighting the difficulty of paleosalinity reconstruction as well as the complexity of the regional hydrology.

Although many SST reconstructions exist for the ETP, using various proxies such as planktonic $\delta^{18}O$, microfossil assemblages or Mg/Ca, few have the resolution necessary to investigate millennial-scale features. Those that have the required resolution focused on the deglaciation, in particular H1 and the YD (Kienast et al., 2006; Pahnke et al., 2007; Koutavas and Sachs, 2008; Kienast et al., 2013), and will be discussed further in paragraph 6.3. Leduc et al. (2007) presented a UK'37-SST record for core MD02-2529 (8°12.33'N, 84°07.32'W; hereafter MD29), which is located close to ME43. The UK'37-SST record of MD29 shows very similar millennial-scale features to the record of ME43, including the cooling events which we observe further south in the Cold Tongue (Fig. 6). Match between the two SST records could be improved even further by carefully aligning the age models, which is beyond the scope of the present manuscript. Note that in this figure, we have applied the Prahl et al. (1988) calibration equation to convert the UK'37 index into SST for both of the records.

Interestingly, Mg/Ca records of high enough resolution do not reveal millennial-scale events typical of the Northern or Southern Hemisphere (e.g. Lea et al., 2006; Pena et al., 2008). One explanation for these discrepancies might be the fact that Mg/Ca records are markedly affected by the preservation of foraminiferal shells (Herbert, 2003; Mekik et al., 2007; Regenberg et al., in press). Another interpretation may be related to potential seasonal sensitivities of Mg/Ca data in the ETP (Sachs, 2008; Timmermann and Timm, 2008) and the fact that in Coupled General Circulation Models the Atlantic/Pacific atmospheric connections is most pronounced during boreal spring (Xie et al. 2008, their Figure 11).

The first long-term (Fig. 5d) and the second deglacial (Fig. 5f) principal components exhibit the key millennial-scale features captured by the northeastern Atlantic UK'37-SST reconstruction of core MD01-2444 (37°33.68′N, 10°08.53′W; Martrat et al., 2007) (Fig 5f, blue line), thus supporting the evidence for an Atlantic/EEP connection. MD01-2444, located off the Iberian Margin, has been chosen here as a template for North Atlantic SST variability representing millennial-scale variability with high enough resolution. Nearby SST records from e.g. the Alboran Sea (Cacho et al., 1999) show very similar features to MD01-2444. We think that anomalously strong northeasterly winds across Central America are the most likely explanation for this Atlantic-Pacific linkage, causing the millennial-scale SST excursions we observe in the ETP. Strong cross-isthmus winds (section 2) would enhance upwelling along the Central American Coast and the southwestward advection of cold water towards the equator.

6.3 Comparison to modeling studies

The prevalent millennial-scale Atlantic/Pacific connection identified here in proxy SST data is also simulated by Coupled General Circulation Models (CGCMs).

Anomalous northeasterly winds across Central America are a feature seen in most CGCMs in response to North Atlantic water hosing experiments (Zhang and Delworth, 2005; Timmermann et al., 2007). These experiments typically show a robust intensification of the gap winds across Central America (Xie et al., 2008), an anomalous anticyclone over the Caribbean, a southward shift of the ITCZ in the tropical Atlantic and ETP and an intensification of the Aleutian Low (Okumura et al., 2009). Enhanced northeasterly trades in the EPWP generate enhanced evaporation, mixing and upwelling and subsequent cooling. This cooling can further spread across the equator via air-sea interactions (Xie et al., 2008), such as the Wind-Evaporation-SST feedback, thus explaining the synchronized temperature changes on millennial timescales seen by the 3 100 kyr long ETP UK’37-SST data sets presented here.

Further south, this surface wind anomaly is responsible for anomalous ocean downwelling. Zhang and Delworth [2005] simulated a cooling of ~1°C north of the equator off the coast of Central America and a warming of ~0.4°C centered around 7°S in the Cold Tongue. Kienast et al. (2013) recently observed such a pattern of SST distribution during the H1 interval, in particular a slight warming in cores V19-28, V19-30 and TR31, which are located south of our three long records (between 2°22’S and 3°35’S, Fig. 5b and c). This dipole pattern is clearly captured in the second deglacial EOF (Fig. 5c). Note that the EOF pattern (positive in the North) has to be multiplied with the negative value of PC2 during Heinrich events to produce the cooling in the North and warming in the South. Results showing the ETP SST difference between strong and weak AMOC simulated by a GFDL CM2.1 idealized waterhosing experiment (Zhang and Delworth 2005, Timmermann et al. 2007) are shown as contours in Fig. 5c.

The limit between cooling and warming in the data set presented by Kienast et al. (2013) for H1 is located ~2°S (cooling in RC11-238 at 1°31'S and warming in V19-28 at 2°22'S). Assuming that the boundary between the warming/cooling during Heinrich events has stayed more or less constant through time, our southernmost core ME27 at 1°51'S would not have experienced the warming predicted by Zhang and Delworth (2005). Unfortunately, none of the published records located further south extends back in time to 100 kyr BP.

Because the deglacial set of cores includes cores south of 2°S (V19-28, V19-30 and TR31) experiencing warming during H1, the amplitude of cooling of the deglacial PC1 during H1 is significantly damped in comparison to the long-term PC1 (Fig. 5d and e). On the other hand, all the other records north of 2°S experience cooling, as expected (Fig. 3). In summary, the deglacial EOF pattern exhibited by ETP UK'37-SST records is consistent with the meridional dipole pattern in the Eastern Pacific simulated by CGCMs in response to North Atlantic AMOC changes (Zhang and Delworth, 2005; Timmerman et al., 2007, Merkel et al. 2010).

7. Conclusions

Over the last 100 kyr, we observe a largely constant temperature offset between the EPWP, the Equatorial Upwelling and the northern Peruvian Upwelling region based on three cores stretching from 8°N and 2°S. This suggests that on orbital time-scales, the dynamics regulating SST affected these three environments uniformly. Superimposed on the glacial-interglacial SST pattern at these sites, we observe abrupt cooling events of up to 2 degrees during most Heinrich events. We suggest that these millennial-scale cooling events are related to cooling in the North Atlantic and the resulting intensification of the Central American gap wind system. Regional upwelling associated with the gap winds likely lead to significant contributions of cold waters originating from the coast of Central America to the equatorial region.

Acknowledgements

Core material was generously provided by the Core Repositories of Oregon State University (supported by NSF grant OCE97-12024) and the University of Rhode Island (supported by NSF grant OCE-9102410). The authors are greatly indebted to A. C. Mix who kindly made available his unpublished benthic $\delta^{18}O$ records of all three cores recovered during the 2000 R/V Melville expedition to the EEP. Thanks are due also to Dr. A. Koutavas for providing his compilation of UK'37-SST records from the eastern tropical Pacific. This contribution benefitted from discussions with A. C. Mix and R. F. Anderson, and from constructive comments by two anonymous journal referees. Claire Normandeau provided invaluable technical assistance. Funding of this study was provided by NSERC Canada (M.K.), the Canadian Institute for Advanced Research (CIFAR; M.K.), the Geological Society of America (GSA; N.D.), the Swiss NSF (SNSF grant PBSKP2-128454 for N.D.), the U.S. NSF (1010869, 1204011 for A.T.) and the Japan Agency for Marine-Earth Science and Technology (A.T).

References

Alexander, M.A., Vimont, D.J., Chang, P., Scott, J.D., 2010. The Impact of Extratropical Atmospheric Variability on ENSO: Testing the Seasonal Footprinting Mechanism

Using Coupled Model Experiments. Journal of Climate 23, 2885–2901.

Alory, G., Maes, C., Delcroix, T., Reul, N. Illig, S., 2012. Seasonal dynamics of sea surface salinity off Panama: The far Eastern Pacific Fresh Pool. J. Geophys. Res. 117, C04028.

Barnett, T., Latif, M., Kirk, E., Roeckner, E., 1991. On ENSO physics. J. Clim. 4, 487–515.

Benway, H.M., Mix, A.C., Haley, B.A., Klinkhammer, G.P., 2006. Eastern Pacific Warm Pool paleosalinity and climate variability: 0-30 kyr. Paleoceanography 21, PA3008.

Caballero, R., Anderson, B.T., 2009. Impact of midlatitude stationary waves on regional Hadley cells and ENSO. Geophysical Research Letters 36, L17704.

Cacho, I., Grimalt, J. O., Pelejero, C., Canals, M., Sierro, F. J., Flores, J. A., Shackleton, N., 1999. Dansgaard-Oeschger and Heinrich event imprints in Alboran Sea paleotemperatures. Paleoceanography, 14, 698-705.

Casey, K.S., Brandon, T.B., Cornillon, P., Evans, R., 2010. "The Past, Present and Future of the AVHRR Pathfinder SST Program", in Oceanography from Space: Revisited, eds. V. Barale, J.F.R. Gower, and L. Alberotanza, Springer.

Chelton, D.B., Freilich, M.H., Esbensen, S.K., 2000. Satellite observations of the wind jets off the Pacific coast of Central America. Part II: Relationships and dynamical considerations. Mon. Weather Rev. 128, 2019–2043.

Drexler, J.W., Rose, W.I.J., Sparks, R.S.J., Ledbetter, M.T., 1980. The Los Chocoyos Ash, Guatemala: a major stratigraphic marker in middle America and in three ocean basins. Quaternary Research 13, 327-345.

Dugdale, R. C. Lyle, M., Wilkerson, F.P., Chai, F., Barbert, R.T., Peng, T.-H., 2004. Influence of equatorial diatom processes on Si deposition and atmospheric CO2 cycles at glacial/interglacial timescales. Paleoceanography 19, PA3011.

Dubois, N., Kienast, M., Kienast, S., Normandeau, C., Calvert, S.E., Herbert, T.D., Mix, A., 2011. Millennial-scale variations in hydrography and biogeochemistry in the Eastern Equatorial Pacific over the last 100 kyr. Quaternary Science Review 30, 210–223.

Dubois, N., Kienast, M., Normandeau, C., Herbert, T.D., 2009. The east equatorial Pacific cold tongue during the last glacial maximum as seen from alkenone paleothermometry. Paleoceanography 24, PA4207.

Fiedler, P.C., 2002. The annual cycle and biological effects of the Costa Rica Dome. Deep Sea Res. Part I 49, 321–338.

Frankenfield, H. C. ‘Northers’’ of the Canal Zone. Mon. Wea. Rev., 45, 546–550 (1917).

Grootes, P. M. & Stuiver, M. Oxygen 18/16 variability in Greenland snow and ice with 10^{-3} to 10^{5}-year time resolution. *J. Geophys. Res.* **102**, 26,455–426,470 (1997).

Herbert, T. D., 2003. Alkenone paleotemperature determinations. Treatise on Geochemistry 6, 391-432.

Hughen, K. A., et al., MARINE04 marine Radiocarbon age calibration, 26-0 ka BP. Radiocarbon 46, 1059-1086 (2004).

Joussaume, S., Sadourney, R., Vignal, C., 1986. Origin of precipitating water in a numerical simulation of the July climate. Ocean–Air Inter. 1, 43–56.

Kaiser, J., F. Lamy and D. Hebbeln (2005), A 70-kyr sea surface temperature record off southern Chile (Ocean Drilling Program Site 1233), Paleoceanography, 20, PA4009.

Kessler, W.S., 2006. The circulation of the eastern tropical Pacific: A review. Prog. Oceanogr. 69, 181–217.

Kessler, W.S., 2002. Mean three-dimensional circulation in the northeast tropical Pacific. Journal of Physical Oceanography 32, 2457–2471.

Kienast, M., MacIntyre, G., Dubois, N., Higginson, S., Normandeau, C., Chazen, C.R., 2012. Alkenone unsaturation in surface sediments from the eastern equatorial Pacific: Implications for SST reconstructions. Paleoceanography 27, PA1210.

Kienast, M., Kienast, S.S., Calvert, S.E., Eglinton, T.I., Mollenhauer, G., François, R., Mix, A.C., 2006. Eastern Pacific cooling and Atlantic overturning circulation during the last deglaciation. Nature 443, 846–849.

Kienast, S. S., M. Kienast, A. C. Mix, S. E. Calvert and R. Francois (2007), Thorium-230 normalized particle flux and sediment focusing in the Panama Basin region during the last 30,000 years., Paleoceanography, 22, PA2213.

Kienast, S., Friederich, T., Dubois, N., Hill, P. S., Timmermann, A., Mix, A. C., Kienast, M., 2013. Near collapse of the meridional SST gradient in the eastern equatorial Pacific during Heinrich Stadial 1. Paleoceanography 28, 1-12.

Koutavas, A., Sachs, J.P., 2008. Northern timing of deglaciation in the eastern equatorial Pacific from alkenone paleothermometry. Paleoceanography 23, PA4205.

Kusch, S., T. I. Eglinton, A. C. Mix and G. Mollenhauer (2010), Timescales of lateral sediment transport in the Panama Basin as revealed by compound-specific radiocarbon ages of alkenones, Earth and Planetary Science Letters, 290, 340-350.

Lea, D. W., D. K. Pak, C. L. Belanger, H. J. Spero, M. A. Hall and N. J. Shackleton, 2006. Paleoclimate histroy of Galapagos surface waters over the last 135,000 yr.

Quaternary Science Reviews 25, 1152-1167.

Leduc, G., Vidal, L., Tachikawa, K., Rostek, F., Sonzogni, C., Beaufort, L., Bard, E., 2007. Moisture transport across Central America as a positive feedback on abrupt climatic changes. Nature 445, 908–911.

Li, T., Philander, S.G.H., 1996. On the annual cycle of the eastern equatorial Pacific. J. Clim. 9, 2986–2998.

Lisiecki, L. E. & Raymo, M. E. A Pliocene-Pleistocene stack of 57 globally distributed benthic $\delta^{18}O$ records. *Paleoceanography* **20**, PA1003 (2005).

Lüthi, D., Le Floch, M., Bereiter, B., Blunier, T., Barnola, J.-M., Siegenthaler, U. Raynaud, D., Jouzel, J., Fischer, H., Kawamura, K., Stocker, T.F., 2008. High-resolution carbon dioxide concentration record 650,000–800,000 years before present. Nature 453, 379–382.

Marchitto, T. M., Lehman, S. J., Ortiz, J. D., Flueckiger, J., van Geen, A., 2007. Marine radiocarbon evidence for the mechanism of deglacial atmospheric CO_2 rise. Science 316, 1456–1459.

Martrat, B., Grimalt, J.O., Shackleton, N.J., de Abreu, L., Hutterli, M.A. and Stocker, T.F., 2007. Four climate cycles of recurring deep and surface water destabilizations on the Iberian margin. Science 317, 502–507.

Merkel, U., M. Prange, and M. Schulz (2010), ENSO variability and teleconnections during glacial times, *Quat. Sci. Rev.*, *29*, 86-100, 10.1016/j.quascirev.2009.11.006.

Mitchell, T.P., Wallace, J.M., 1992. The annual cycle in equatorial convection and sea surface temperature. J. Clim. 5, 1140–1156.

Okazaki, Y., Timmermann, A., Menviel, L., Harada, N., Abe-Ouchi, A., Chikamoto, M.O., Mouchet, A., Asahi, H., 2010. Deepwater Formation in the North Pacific During the Last Glacial Termination. Science 329, 200–204.

Okumura, Y.M., Deser, C., Hu, A., Timmermann, A. and Xie, S.P., 2009. North Pacific Climate Response to Freshwater Forcing in the Subarctic North Atlantic: Oceanic and Atmospheric Pathways. Journal of Climate 22, 1424–1445.

Pahnke, K., Sachs, J.P., Keigwin, L., Timmermann, A., Xie, S.P., 2007. Eastern tropical Pacific hydrologic changes during the past 27,000 years from D/H ratios in alkenones. Paleoceanography 22, PA4214.

Pak, H., Zaneveld, J.R.V., 1974. Equatorial Front in the Eastern Pacific Ocean. Journal of Physical Oceanography 4, 570–578.

Pena, L. D., I. Cacho, P. Ferretti and M. A. Hall, 2008. El Nino–Southern Oscillation–like variability during glacial terminations and interlatitudinal teleconnections. Paleoceanography 23, PA3101.

Prahl, F.G., Muehlhausen, L.A., Zahnke, D.L., 1988. Further evaluation of longchain alkenones as indicators of paleoceanographic conditions. Geochim. Cosmochim. Acta 52, 2303–2310.

Prange, M., S. Steph, M. Schulz and L. D. Keigwin, 2010. Inferring moisture transport across Central America: Can modern analogs of climate variability help reconcile paleosalinity records? Quaternary Science Reviews 29, 1317-1321.

Regenberg, M., Regenberg, A., Garbe-Schönberg, D. and D. W. Lea, in press. Global dissolution effects on planktonic foraminiferal Mg/Ca ratios controlled by the calcite-saturation state of bottom waters, Paleoceanography.

Reimer, P. J., E. Bard, et al. (2013), IntCal13 and Marine13 Radiocarbon Age Calibration

Curves 0–50,000 Years cal BP, Radiocarbon, 55, 1869-1887.

Richter, I., Xie, S.P., 2010. Moisture transport from the Atlantic to the Pacific basin and its response to North Atlantic cooling and global warming. Climate Dynamics 35, 551–566.

Sachs, J. P. (2008). Divergent trends in Holocene SSTs derived from alkenones and Mg/Ca in the Equatorial Pacific. AGU Fall Meeting 2008. San Francisco.

Schultz, D.M., Bracken, W.E., Bosart, L.F., Hakim, G.J., Bedrick, M.A., Dickinson, M.J., Tyle, K.R., 1997. The 1993 Superstorm Cold Surge: Frontal Structure, Gap Flow, and Tropical Impact. Mon. Weather Rev. 125, 5–39.

Schultz, D.M., Bracken, W.E., Bosart, L.F., 1998. Planetary- and Synoptic-Scale Signatures Associated with Central American Cold Surges. Mon. Weather Rev. 126, 5–27.

Shackleton, N. J., Hall, M. A. & Vincent, E. Phase relationships between millennial-scale events 64,000-24,000 years ago. *Paleoceanography* **15**, 565–569 (2000).

Singarayer, J.S., Richards, D.A., Ridgwell, A., Valdes, P. J., Austin, W.E.N., Beck, J.W., 2008. An oceanic origin for the increase of atmospheric radiocarbon during the Younger Dryas. Geophys. Res. Lett. 35, L14707.

Stuiver, M., Reimer, P.J., 1993 Extended 14C database and revised CALIB radiocarbon calibration program. Radiocarbon 35, 215–230.

Timmermann, A., Okumura, Y., An, S.-I., Clement, A., Dong, B., Guilyardi, E., Hu, A., Jungclaus, J.H., Renold, M., Stocker, T.F., Stouffer, R.J., Sutton, R., Xie, S.-P., Yin, J., 2007. The influence of a weakening of the Atlantic meridional overturning circulation on ENSO. Journal of Climate 20, 4899–4919.

Timmermann, A. and O. Timm (2008). Mechanisms for deglacial temperature rise in the tropical Pacific. AGU Fall Meeting 2008. San Francisco.

Vimont, D.J., Wallace, J.M., Battisti, D.S., 2003. The seasonal footprinting mechanism in the Pacific: Implications for ENSO. Journal of Climate 16, 2668–2675.

Willett, C.S., Leben, R., Lavin, M.F., 2006. Eddies and mesoscale processes in the eastern tropical Pacific: A review. Progress in Oceanography 69, 218–238.

Wyrtki, K., 1981. An estimate of equatorial upwelling in the Pacific. Journal of Physical Oceanography 11, 1205–1214.

Wyrtki, K., 1996. Oceanography of the eastern equatorial Pacific Ocean. Oceanography and Marine Biology. An Annual Review 4, 33–68.

Xie, S.P., Okumura, Y., Miyama, T., Timmermann, A., 2008. Influences of Atlantic climate change on the tropical Pacific via the Central American Isthmus. Journal of Climate 21, 3914–3928.

Xie, S.P., Xu, H.M., Kessler, W.S., Nonaka, M., 2005. Air-sea interaction over the eastern Pacific warm pool: Gap winds, thermocline dome, and atmospheric convection. Journal of Climate 18, 5–20.

Zhang, R., Delworth, T., 2005. Simulated tropical response to a substantial weakening of the Atlantic thermohaline circulation. Journal of Climate 18, 1853–1860.

Figure captions

Figure 1. (a) Relief of the Central American Isthmus with core locations (white dots) and approximate location of low-level wind-jets (gaps winds, purple arrows). Climatological QuikScat wind vectors (2000/01 - 2008/12 inclusive) show wind

direction and speed for March (a) and September (b). QuikScat data are produced by Remote Sensing Systems and sponsored by the NASA Ocean Vector Winds Science Team. Data are available at www.remss.com. The lower panels show mean monthly SST for March (c) and September (d) based on satellite estimates (AVHRR Pathfinder Version 5.0 data; Casey et al., 2010). Numbers next to core sites in (c) show the leading long-term EOF1 pattern.

Figure 2. Benthic δ^{18}O records (*Uvigerina peregrina*) and LR04 stack (Lisiecki and Raymo, 2005) for (a) core ME43 on its original age scale (Benway et al., 2006), (b) core ME43 (c) core ME24 and (d) core ME27 on age scales as updated in this study. Black triangles indicate AMS-14C dates, black circles indicate benthic tie-points and grey bars indicate the Los Chocoyos Ash Layer (Drexler et al., 1980).

Figure 3. Original UK'37-SST time series used for the deglacial EOF. Data for core ME24 are from Kienast et al. (2006). Data for core JPC32-14 are from Pahnke et al. (2007). Data for core MD29 are from Leduc et al. (2007). Data for cores V19-27, V19-28, V19-30, V21-30 and RC11-238 are taken from Koutavas and Sachs (2008). Data for cores ME27, ME43 and TR31 are from Dubois et al. (2009).

Figure 4. Downcore reconstruction of UK'37-SST of the three cores versus age for the last 100 kyr. From top to bottom: (a) Greenland NGRIP δ^{18}O temperature record. (b) ME43 UK'37-SST (original and 15-pt smoothed). (c) ME24 UK'37-SST (original and 15-pt smoothed). (d) ME-27 UK'37-SST (original and 15-pt smoothed). (e) The

principal component corresponding to the leading long-term EOF1. (f) Sea surface temperature difference (ΔSST) between ME43 and ME24. (g) ΔSST between ME43 and ME27. (h) ΔSST between ME24 and ME27. The dashed horizontal line in (h) represents the propagated analytical error above which the ΔSST is significant. The color shading in (b), (c) and (d) represent the analytical error. Grey vertical intervals mark the glacial stages MIS2 and 4, as indicated on the top of the figure. Dashed vertical lines mark the North Atlantic ice rafting and melt-water events: Younger Dryas (YD), Heinrich events (H1–H6).

Figure 5. Leading modes of SST variability: The upper (lower) panels show the patterns (principal components) of the EOF modes of UK'37-SST reconstructions from ETP cores. (a) EOF analysis based on SST reconstructions (5-100 kyr BP) from cores ME24, ME27, ME43. (b) and (c) 1st and 2nd EOF analysis based on the 25-5 kyr BP section of cores V19-27, V19-28, V19-30, V21-30, RC11-238, MD02-2529, JPC32-14, ME24, ME43, ME27 and TR31 (Kienast et al., 2006; Leduc et al., 2007; Pahnke et al., 2007; Koutavas and Sachs, 2008; Dubois et al., 2009; Dubois et al., 2011; Kienast et al., 2013). The contour lines represent SST anomalies from a climate model experiment conducted with the GFDL CM2.1 model (Timmermann et al., 2007), representing present-day control run (100 year mean) minus the AMOC off case (100 year mean). (d) The principal component corresponding to the leading long-term EOF (red) and the UK'37-SST reconstruction from the eastern North Atlantic core MD01-2444 (Martrat et al., 2007; blue). (e) The principal component corresponding to the leading deglacial EOF (red), along with equatorial insolation during October,

November, December (OND, normalized; orange dashed) and atmospheric CO_2 (Lüthi et al., 2008; blue). (f) The principal component corresponding to the second deglacial EOF (red), along with UK'37-SST reconstruction from eastern North Atlantic core MD01-2444 (Martrat et al., 2007; blue).

Figure 6. Comparison of the UK'37-SST from ME43 and MD29 (Leduc et al., 2007), both located in the Panama Basin.

***Highlights (for review)**

1. Millennial-scale cooling events occur in the East Pacific during Heinrich events
2. N. Atlantic SST anomalies affect Central American gap winds and thus the E. Pacific
3. Hydrographic conditions were similar during glacial and interglacial periods.

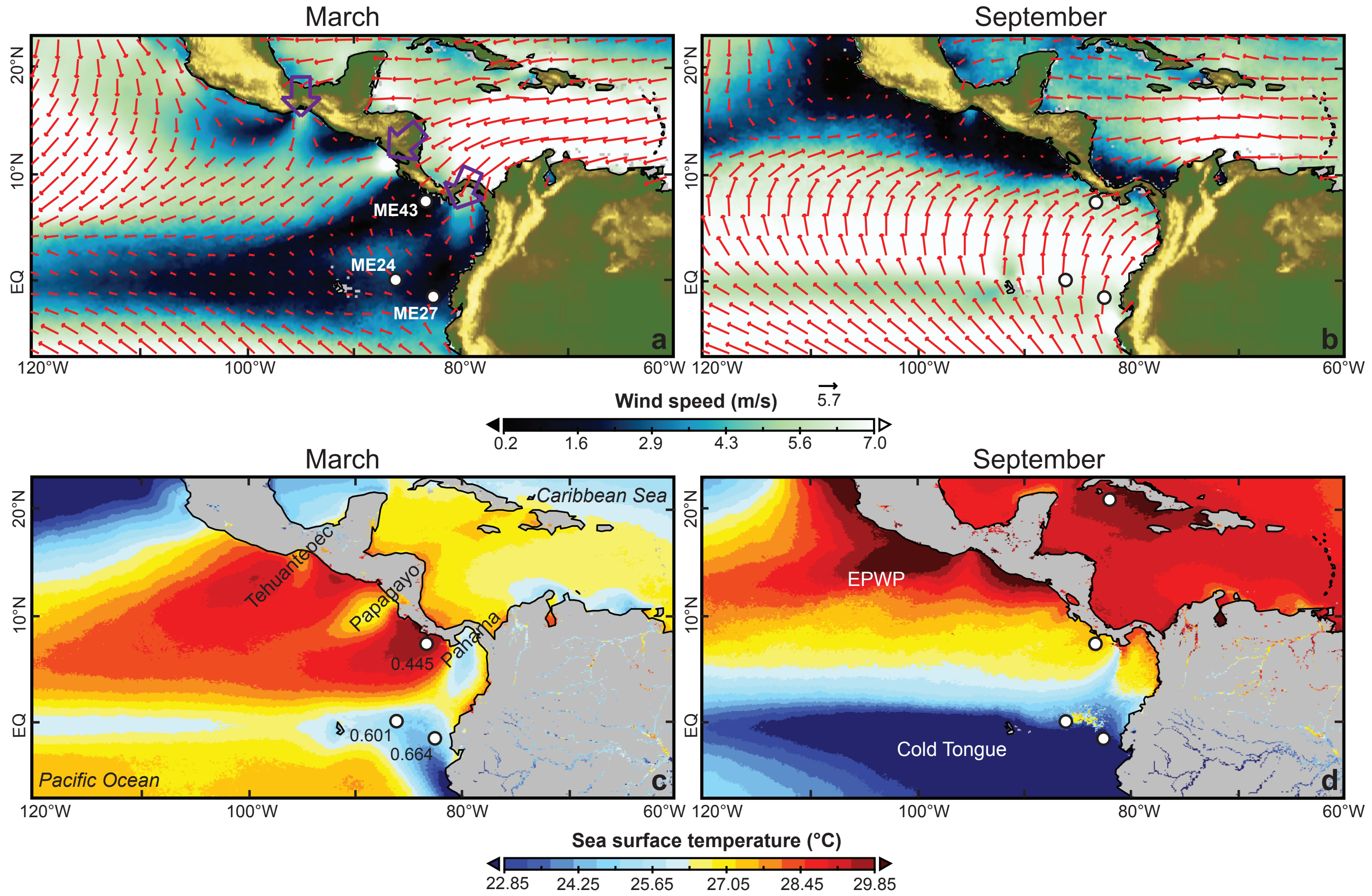
March
September
20°N
10°N
EQ
ME43
ME24
ME27
a
b
120°W
100°W
80°W
60°W
5.7
Wind speed (m/s)
0.2
1.6
2.9
4.3
5.6
7.0
Caribbean Sea
Tehuantepec
Papagayo
Panama
0.445
0.601
0.664
Pacific Ocean
c
EPWP
Cold Tongue
d
Sea surface temperature (°C)
22.85
24.25
25.65
27.05
28.45
29.85

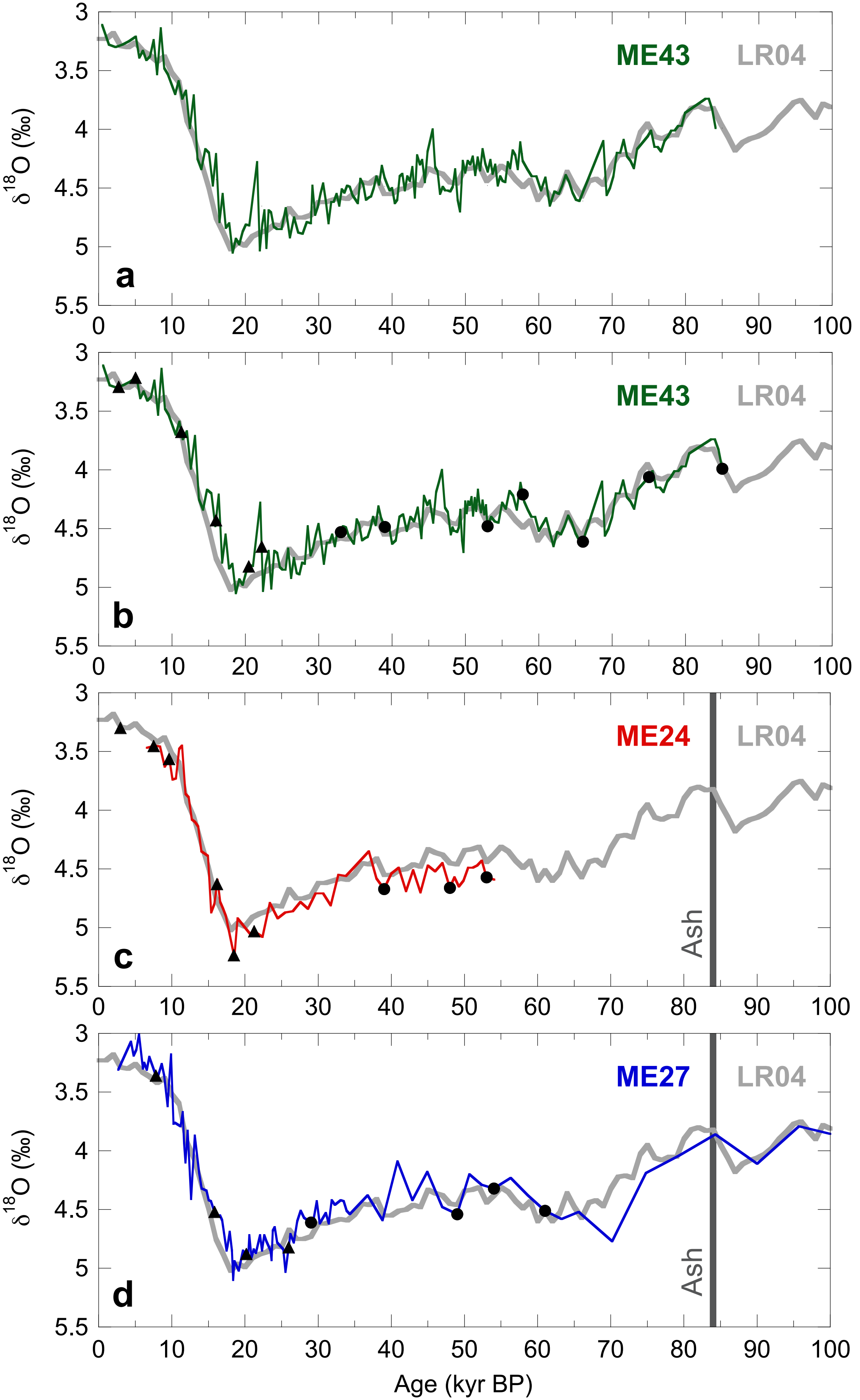
ME43
LR04
a
ME43
LR04
b
ME24
LR04
c
Ash
ME27
LR04
d
Ash
δ18O (‰)
Age (kyr BP)
3
3.5
4
4.5
5
5.5
0
10
20
30
40
50
60
70
80
90
100

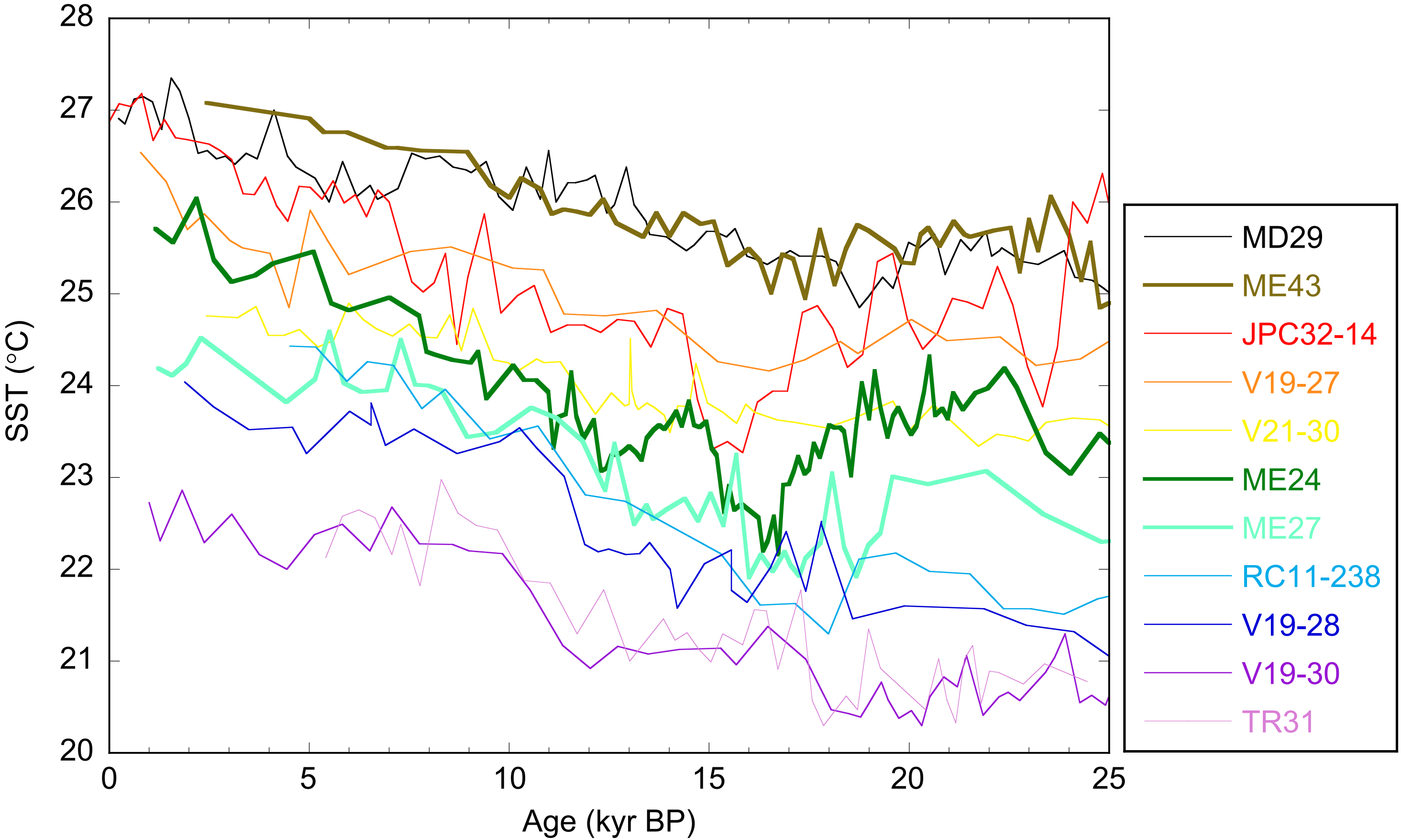

28
27
26
25
24
23
22
21
20
SST (°C)
0
5
10
15
20
25
Age (kyr BP)
MD29
ME43
JPC32-14
V19-27
V21-30
ME24
ME27
RC11-238
V19-28
V19-30
TR31

Figure 4

Click here to download Figure: Dubois_Fig4.pdf

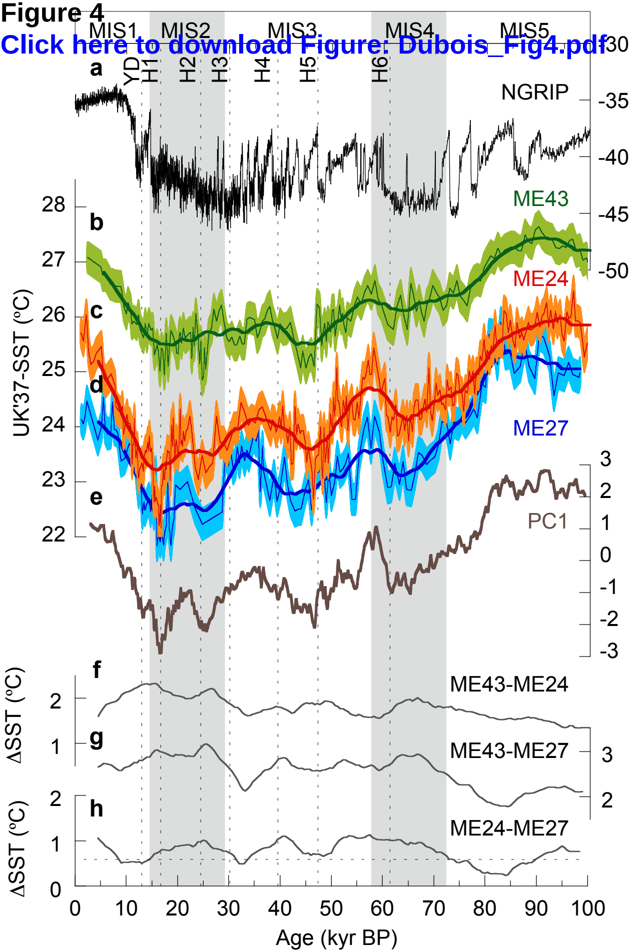

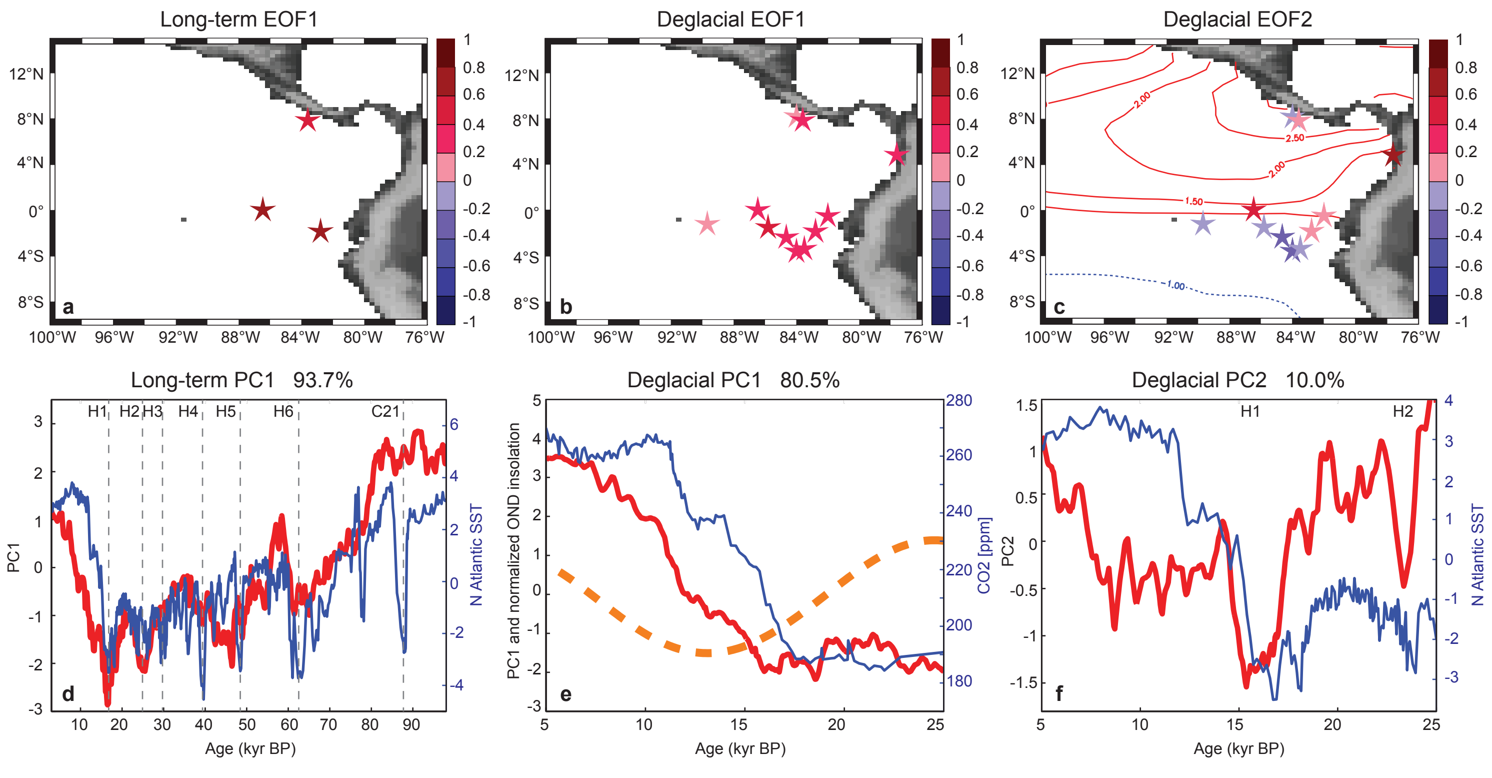

Long-term EOF1
Deglacial EOF1
Deglacial EOF2
12°N
8°N
4°N
0°
4°S
8°S
100°W
96°W
92°W
88°W
84°W
80°W
76°W
a
b
c
2.00
2.50
1.50
-1.00
1
0.8
0.6
0.4
0.2
0
-0.2
-0.4
-0.6
-0.8
-1
Long-term PC1 93.7%
Deglacial PC1 80.5%
Deglacial PC2 10.0%
H1
H2
H3
H4
H5
H6
C21
PC1
N Atlantic SST
d
Age (kyr BP)
PC1 and normalized OND insolation
CO2 [ppm]
e
PC2
f

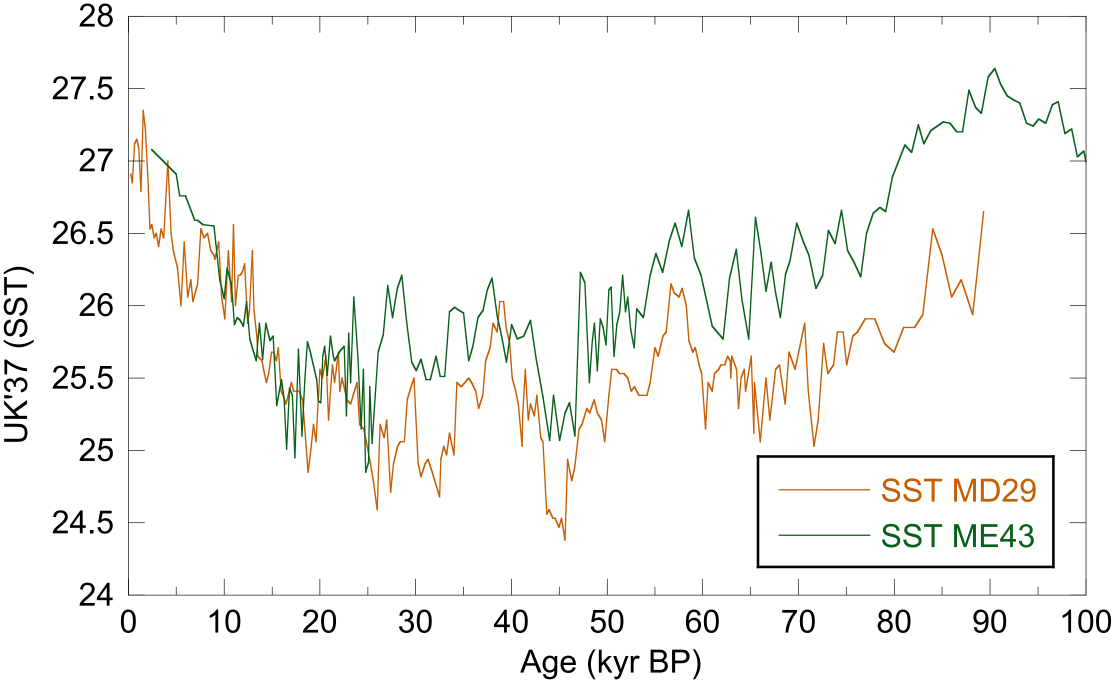

28
27.5
27
26.5
26
25.5
25
24.5
24
UK'37 (SST)
0
10
20
30
40
50
60
70
80
90
100
Age (kyr BP)
SST MD29
SST ME43

Table 1
Click here to download Table: Dubois_Table1.xlsx

Table 1. AMS-^{14}C data

Core	Depth [cm]	^{14}C Age [kyr]	SD [kyr]	Calendar Age [kyr]	SD [kyr]	Species
ME-24	17.5	3.26	0.03	2.99	0.06	*N. dutertrei*
ME-24	48.5	7.10	0.04	7.52	0.04	*N. dutertrei*
ME-24	81	9.04	0.04	9.62	0.06	*N. dutertrei*
ME-24	230	13.90	0.04	16.16	0.08	*N. dutertrei*
ME-24	291	15.70	0.09	18.50	0.11	*N. dutertrei*
ME-24	351	18.05	0.07	21.24	0.14	*N. dutertrei*
ME-27	41	7.43	0.04	7.83	0.05	*N. dutertrei*
ME-27	91	13.65	0.07	15.84	0.12	*N. dutertrei*
ME-27	120	17.20	0.07	20.18	0.11	*N. dutertrei*
ME-27	160	22.20	0.10	25.97	0.09	*N. dutertrei*
ME-43	13	3.10	0.04	2.80	0.04	*N. dutertrei*
ME-43	26	4.94	0.04	5.18	0.08	*N. dutertrei*
ME-43	91	10.45	0.06	11.46	0.15	*N. dutertrei*
ME-43	131	13.70	0.08	15.90	0.13	*N. dutertrei*
ME-43	186	17.90	0.10	21.04	0.16	*N. dutertrei*
ME-43	208	19.15	0.11	22.54	0.12	*N. dutertrei*

Table 2
Click here to download Table: Dubois_Table2.xlsx

Table 2. Age models as updated in this study

Depth (cm)	Age (kyr BP)	Dating method
ME43: Age model published by Benway et al. (2006)		
13	2.68	radiocarbon MARINE04
26	5.06	radiocarbon MARINE04
91	11.39	radiocarbon MARINE04
131	15.56	radiocarbon MARINE04
186	20.51	radiocarbon MARINE04
208	22.12	radiocarbon MARINE04
228	23.30	planktic O18 strat. (tied to GISP2)
238	24.00	planktic O18 strat. (tied to GISP2)
281	28.94	planktic O18 strat. (tied to GISP2)
286	29.14	benthic O18 strat (tied to MD95-2045)
421	38.97	benthic O18 strat (tied to MD95-2045)
516	45.53	benthic O18 strat (tied to MD95-2045)
696	57.81	benthic O18 strat (tied to MD95-2045)
736	62.74	benthic O18 strat (tied to MD95-2045)
956	83.18	benthic O18 strat (tied to MD95-2045)
ME43: Age model as updated in this study		
13	2.72	radiocarbon MARINE13
26	5.04	radiocarbon MARINE13
91	11.26	radiocarbon MARINE13
131	15.99	radiocarbon MARINE13
186	20.47	radiocarbon MARINE13
208	22.23	radiocarbon MARINE13
386	33.00	benthic O18 strat. (tied to LR04)
465	39.00	benthic O18 strat. (tied to LR04)
642	53.00	benthic O18 strat. (tied to LR04)
696	57.81	benthic O18 strat. (tied to LR04)
770	66.00	benthic O18 strat. (tied to LR04)
871	75.00	benthic O18 strat. (tied to LR04)
966	85.00	benthic O18 strat. (tied to LR04)
ME24: Age model as updated in this study		
17.5	2.99	radiocarbon MARINE13
48.5	7.52	radiocarbon MARINE13
81	9.62	radiocarbon MARINE13
230	16.16	radiocarbon MARINE13
291	18.50	radiocarbon MARINE13
351	21.24	radiocarbon MARINE13
522	39.00	benthic O18 strat. (tied to LR04)
612	48.00	benthic O18 strat. (tied to LR04)
692	53.00	benthic O18 strat. (tied to LR04)
980	84.00	Ash layer (min in CaCO3)
ME27: Age model as updated in this study		
41	7.83	radiocarbon MARINE13
91	15.84	radiocarbon MARINE13
120	20.18	radiocarbon MARINE13
160	25.97	radiocarbon MARINE13
173	29.00	benthic O18 strat. (tied to LR04)
271	49.00	benthic O18 strat. (tied to LR04)
301	54.00	benthic O18 strat. (tied to LR04)
331	61.00	benthic O18 strat. (tied to LR04)
431	84.00	Ash layer (min in CaCO3)
522	110.00	benthic O18 strat. (tied to LR04)

Table 3
Click here to download Table: Dubois_Table3.xlsx

Table 3. List of cores used in the deglacial EOF computation

Core name	Location		Depth	degl.	degl.	References
	Lat.	Long.	(m)	EOF1	EOF2	
MD29	8°12'N	84°07'W	1619	0.1974	-0.1751	Leduc et al. (2007)
ME43	7°51'N	83°36'W	1368	0.231	0.0126	Dubois et al. (2009)
JPC32-14	4°39'N	77°57'W	2200	0.2139	0.777	Pahnke et al. (2006)
ME24	0°01'N	86°27'W	2941	0.2754	0.4135	Kienast et al. (2006)
V19-27	0°28'S	82°40'W	1373	0.2277	0.0504	Koutavas & Sachs (2008)
ME27	1°51'S	82°47'W	2203	0.3117	0.0996	Dubois et al. (2009)
V21-30	1°13'S	89°41'W	617	0.206	-0.0573	Koutavas & Sachs (2008)
RC11-238	1°31'S	85°49'W	2573	0.4787	-0.0585	Koutavas & Sachs (2008)
V19-28	2°22'S	84°39'W	2720	0.3987	-0.2706	Koutavas & Sachs (2008)
V19-30	3°23'S	83°31'W	3091	0.326	-0.1896	Koutavas & Sachs (2008)
TR31	3°37'S	83°58'W	3209	0.3167	-0.2572	Dubois et al. (2009)